

Joint Liver and Hepatic Lesion Segmentation using a Hybrid CNN with Transformer Layers

Georg Hille, Shubham Agrawal, Christian Wybranski, Maciej Pech, Alexey Surov, Sylvia Saalfeld

Abstract—Deep learning-based segmentation of the liver and hepatic lesions therein steadily gains relevance in clinical practice due to the increasing incidence of liver cancer each year. Whereas various network variants with overall promising results in the field of medical image segmentation have been developed over the last years, almost all of them struggle with the challenge of accurately segmenting hepatic lesions. This led to the idea of combining elements of convolutional and transformer-based architectures to overcome the existing limitations. This work presents a hybrid network called SWTR-Unet, consisting of a pretrained ResNet, transformer blocks as well as a common Unet-style decoder path. This network was applied to clinical liver MRI, as well as to the publicly available CT data of the liver tumor segmentation (LITS) challenge. Additionally, multiple state-of-the-art networks were implemented and applied to both datasets, ensuring a direct comparability. Furthermore, correlation analysis and an ablation study were carried out, to investigate various influencing factors on the segmentation accuracy of our presented method. With Dice similarity scores of averaged $98 \pm 2\%$ for liver and $81 \pm 28\%$ lesion segmentation on the MRI dataset and $97 \pm 2\%$ and $79 \pm 25\%$, respectively on the CT dataset, the proposed SWTR-Unet outperforms each of the additionally implemented state-of-the-art networks. The achieved segmentation accuracy was found to be on par with manually performed expert segmentations as indicated by inter-observer variabilities for liver lesion segmentation. In conclusion, the presented method could save valuable time and resources in clinical practice.

Index Terms—deep learning, hepatic lesions, hybrid architecture, segmentation, multi-modal

I. INTRODUCTION

Following cardiovascular diseases, cancer constitutes, with approximately 8.8 million deaths globally in 2015 the second major cause of death, with the liver as one of the most common sites to develop primary and metastatic lesions [1]. With regards to diagnosis and disease progression, abnormal shapes and textures of the liver, as well as present lesions visible in medical imaging represent relevant biomarkers [2].

This work is partly funded by the Federal Ministry of Education and Research within the Forschungscampus *STIMULATE* (grant no. 13GW0473A).

Georg Hille, Shubham Agrawal, and Sylvia Saalfeld: Department of Simulation and Graphics, Otto-von-Guericke University, Magdeburg, Germany. (e-mail: georg.hille@ovgu.de)

Georg Hille and Sylvia Saalfeld: Forschungscampus *STIMULATE*, Magdeburg, Germany.

Christian Wybranski, Maciej Pech, Alexey Surov: Department of Radiology, University Hospital of Magdeburg, Magdeburg, Germany.

Besides metastatic lesions, which often originate from primary breast, colon and pancreas cancer, the liver is also site of primary tumor development [3]. The Hepatocellular carcinoma (HCC) is among the most frequent tumor variants and causes the third-most cancer-related deaths worldwide with a growing incidence over the last decades [3]. In terms of diagnosis and therapy planning, medical imaging of the liver plays a vital role, either during the routinely performed tumor staging of primary lesions outside of the liver or if the clinical anamnesis points towards primary hepatic cancer diseases. For such imaging purposes, computed tomography (CT) and magnetic resonance imaging (MRI) are obligatory. While CT offers high spatial resolution and minimal susceptibility for motion artifacts due to fast acquisition times, the major drawbacks lie in the radiation exposure and the inferior soft tissue contrast compared to MRI. The latter enables freely adjustable cross-section angles and varying tissue contrasts due to multiple acquisition sequences, which pronounce different physiological tissue compositions. These advantages come with the cost of time-consuming acquisition procedures, which commonly limit the overall spatial resolution and are prone to multiple image artifacts, e.g., motion or bias artifacts.

The precise identification and segmentation of hepatic lesions in CT and MR images could support radiologists in tumor staging and therapy decision-making. In current clinical routine it is common that such segmentation procedures are performed manually, which represents the gold standard or semi-automatically with algorithmical support. Either way, both strategies and particularly manually contouring, are time-consuming, cumbersome, operator-dependent and subjective. Even more automatized approaches, which have been developed in the past, require manual initialization and their segmentation accuracy often heavily rely on the precision of such initial user interactions. Due to the above mentioned limitations, there is still a need for fully automatic segmentation approaches. However, it has been shown that precisely segmenting hepatic lesions is a highly challenging task due to the vast variability of shape, texture, size, location and number of liver tumors per patient case. The tissue image contrast between liver and lesion highly varies depending on the used acquisition protocols or the application of contrast-agents and thus, it is hardly possible to define a model-based segmentation approach based on crafted features by a priori knowledge. Such approaches include graph cuts, level sets or clustering techniques, that have been applied almost exclusively to liver CT data [4]–[6]. With respect to the imaging modality, the

same holds true for machine or deep learning-based methods, which were almost exclusively applied to liver CT images. Nevertheless, learning-based approaches seem to be the most promising strategy to deal with the sheer appearance complexity of such liver lesions. In recent years various works focused on CT-based liver and liver lesion segmentation, especially since the liver tumor segmentation (LiTS) challenge publicly provided patient CT scans, which are otherwise hard to compromise in reasonable numbers. In terms of MRI-based hepatic lesions segmentation, there currently is, to the best of the authors' knowledge, only the work of Christ et al. [7] of direct relevance. They presented a fully automatic approach consisting of a cascaded convolutional neural network (CNN), that first segments the liver outline and subsequently the hepatic lesions within the resulting liver mask images. Christ et al. [7] applied their two-step strategy to both, liver CT and a few MR images and achieved averaged liver Dice similarity scores of 94% (CT) and 87% (MRI), as well as lesion Dice similarity scores on average of 61% (CT) and 69.7% (MRI). Their used dataset was comprised of 100 CT patient scans and thereof 20 validation cases as well as 31 MRI scans without any details about the validation set size. In contrast to MRI-based hepatic lesion segmentation, various works dealing with CT imaging have been presented in recent years. Both, Unet-style architectures processing 2D image input like [8]–[10] and 3D-based approaches like [11], [12] and even hybrid variants, which combine 2D and 3D components [13] have been applied to this particular segmentation task. A more recent work from Fan et al. [14] introduced attention mechanisms, originated from the computer vision domain and included such block-wise elements within a common CNN-architecture. Although, all of these works achieved liver segmentation accuracies of $> 90\%$ and most of them even $> 95\%$ Dice, they commonly lack sufficient segmentation quality regarding the hepatic lesions, which therefore represents and remains the primary challenge.

The aim of this work was to develop a fully automatic deep learning-based joint liver and hepatic lesion segmentation approach with the capability of expert-like segmentation accuracy, that could be applied to both, clinical MRI and CT data. Furthermore, to ensure a mere direct comparability of the proposed method with relevant works from the state of the art, multiple network variants were additionally implemented and tested on the same imaging data.

II. MATERIALS AND METHODS

Figure 1 shows the architecture of the proposed SWTR-Unet (SWIN-Transformer-Unet) network for liver and hepatic lesion segmentation in MRI and CT. The SWTR-Unet combines various elements of current state-of-the-art architectures and fuses them into a hybrid network consisting of convolutional and transformer-based elements. In that regard Res-blocks, transformer-based multi-head self-attention (MSA) blocks as well as shifting window (SWIN) transformer blocks were included. The components of the SWTR-Unet will be described in more detail in the following.

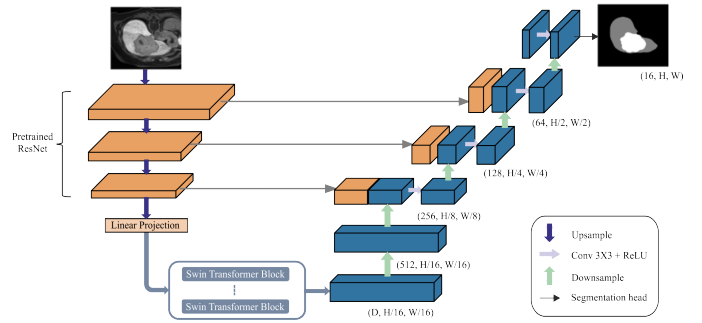


Fig. 1. The basic architecture of the proposed hybrid SWTR-Unet, that combines a ResNet-styled encoder path, transformer blocks at the Unet-bottleneck and a common convolutional decoder path.

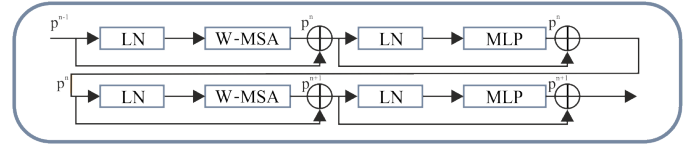


Fig. 2. Structure of a SWIN-transformer block proposed by Cao et al. [27] consisting of a sequence of LayerNorm (LN) layers, window-based multi-head self-attention (W-MSA) or shifted window-based multi-head self-attention (SW-MSA) blocks and multilayer perceptrons (MLP).

A. SWTR-Unet

Regarding the hybrid encoder design of the proposed network a ResNet [15] was implemented as a convolutional backbone, which was pretrained on ImageNet [16] and combined with in total 12 transformer blocks at the bottleneck of the Unet. Beside the function as a robust feature extractor, the Res-blocks within the pretrained ResNet also address the vanishing gradient problem and allow a more dynamic and efficient learning [15]. Fully convolutional-based networks like the widely known and applied Unet commonly suffer from the limitation of capturing long-term dependencies due to the intrinsic locality of convolutional operations. For extracting the global contextual information, the transformer elements encode the input images as a sequence of image patches. Then, the decoder performs the upsampling task needed for retrieving the precise localization [17]. The transformer architecture employs dispense convolution operators and relies on a multi-head self-attention mechanism instead. The 12 transformer layers in the SWTR-Unet consist of multiple consecutive SWIN-transformer sub-blocks. Each of those sub-block comprises layer normalization (LN), multi-headed self-attention (MSA) modules, residual connections, and a 2-layer multilayer perceptron (MLP) with a Gaussian Error Linear Unit (GELU) activation for adding non-linearity to the network. Regarding the self-attention modules, window-based multi-headed self-attention (W-MSA) and shifted window-based multi-headed self-attention (SW-MSA) are successively applied.

The input for the SWIN-transformer blocks as the Unet bottleneck is generated by the preceding linear projection layer, which reshapes the 2D image in a sequence of 2D image tokens or patches, respectively of size 16×16 pixels [18]. The transformer architecture conducts global self-attention by computing the relationship of each patch with all other

patches of the fed sequence, resulting in a computation of quadratic complexity [19]. This would make global self-attention mechanisms unsuitable for larger images. In order to overcome this limitation, shifted window-based local self-attention as proposed by Vaswani et al. [19], could reduce the computational costs due to linear complexity and furthermore, introduce cross-window connections via shifting.

The final segmentation masks of liver and lesions are obtained by the decoder-path of the STWR-Unet, which consists of in total four up-sampling layers. Starting at the bottom of the Unet-style architecture, the sequence of hidden features as output of the transformer blocks, is reshaped and then successively led through the decoder layers, where each consists of a two-times upsampling layer, a 3×3 convolutional layer and a Rectified linear unit (ReLU) layer. Therefore, the proposed SWTR-Unet is capable of aggregating both, local and global features as present in different resolution levels by preserving and transferring them to the decoder side via skip connections. Finally, the feature map is passed through the segmentation head to generate the segmentation output.

B. Imaging Data

Since both, CT and MR imaging are of crucial importance in clinical routine of hepatic lesion diagnosis and treatment decision-making, the same pipeline of pre-processing, training and evaluation was used with the data both imaging modalities.

The MR imaging data were retrospectively compiled and originally used for intervention planning purposes before brachytherapy at the Department of Radiology and Nuclear Medicine of the University Hospital in Magdeburg. The images were acquired using a Philips Intera 1.5 T scanner and an eTHRIVE sequence with repetition (TR) and echo times (TE) of 4.0 - 4.1 ms and 2.0 ms, respectively. In-plane image resolution of the axial scans was 0.98 mm, the spacing between slices was 3 mm, resulting in acquisition matrices of size $224 \times 224 \times 64$. A total of 48 patient cases with overall 157 hepatic lesions were compiled. The ground truth segmentations of the liver outline and the hepatic lesions therein were performed by an experienced radiologist.

With respect to CT imaging, the LiTS challenge [20] data was used, which comprises scans from several clinical sites, using different acquisition protocols and CT scanners, and thus, the image quality and resolution vary noticeably. In-plane image resolution of the axial scans varies from 0.56 mm to 1.0 mm and the slice thickness varies from 0.45 mm to 6.0 mm. The number of slices per volume ranges from 42 to 128 [21]. The hepatic lesions, that are present in each patient scan vary in size between 38 mm^3 and 349 cm^3 [21].

C. Pre-processing and Augmentation

The following description of the data pre-processing and augmentation holds true for both the MRI and CT data, if not stated otherwise. First, adaptive histogram equalization was performed to enhance the contrast volume-wise followed by resampling to a fixed matrix size. With regard to the MRI data, z-score normalization was performed, followed by a N4 bias correction. For CT data, the Hounsfield units

were limited to the range $[-100; 400]$ to exclude irrelevant outlier pixel intensities and subsequently normalized using the 5th and 95th percentile of the foreground intensities. Data augmentation consisting of various intensity and geometrical approaches were employed to strengthen the network's robustness and generalization ability, since the number of available patient cases was relatively small, especially compared to the amount of trainable parameters of the network. The image data was augmented using the application of Gaussian noise, gamma and affine transformations, including flipping (overall probability of 60%, for each direction 50%), rotation ($\pm 20^\circ$) and translation (± 32 voxels for the x and y-axis and ± 16 voxels for the z-axis). Each of the 48 volumes of the MRI dataset was augmented 20-times leading to 960 samples of size $224 \times 224 \times 64$ voxels. Analogous, the 131 CT volumes were augmented 20-times and yielded in total 2,620 samples. Both, datasets were split into single slices for 2D image input, resulting in a total of 61,440 MR and 189,600 CT images.

D. Implementation details

The implementation of the proposed SWTR-Unet as well as relevant state-of-the-art methods based on Python 3.6 and Pytorch 1.7.0. All of the models were trained on a NVIDIA GeForce RTX2080 Ti GPU with 12GB of memory. Due to the limitation of GPU memory, the used batch size was 32 for 2D input and 8 in the case of the 3D input of the DAF3D network [22]. Table I describes the hyperparameter used after fine-tuning for each of the experimented methods.

In order to evaluate the capability of the methods listed in Table I to segment the liver and lesions therein, 7-fold-cross validation was performed. Therefore, the MR dataset was separated into seven subsets each containing the augmented data of 41 to 42 image volumes for training purposes as well as six to seven original volumes within a corresponding validation set. Similarly, the CT data set is separated into seven-fold, each containing the augmented data of 114 image volumes for training purposes as well as 17 original volumes within a corresponding validation set. In doing so, it is guaranteed that the networks produce segmentation masks on unseen images with respect to the training process per fold. The 2D networks were applied to all slices per validation volume and predicted 2D slices were subsequently combined patient-wise to calculate the quality metrics regarding the segmentation accuracy per patient image volume. The results stated in the following refer to the average over all seven folds.

E. Quality metrics

In order to assess and compare the capability of liver and hepatic lesion segmentation of the proposed SWTR-Unet with the state-of-the-art networks, Dice similarity coefficients and Hausdorff distances were used. The former is defined as

$$DSC = \frac{2|X \cap Y|}{|X| + |Y|}, \quad (1)$$

where $|X|$ and $|Y|$ represent the reference and the resulting network's segmentation. The Hausdorff distance, also known as the maximum surface distance, is defined as:

TABLE I

HYPERPARAMETER SETTINGS FOR EACH OF THE IMPLEMENTED NETWORKS, BOTH STATE-OF-THE-ART ARCHITECTURES AND OUR PROPOSED SWTR-UNET VARIANT. THE CENTER LINE SEPARATES PURE CONVOLUTIONAL NETWORKS FROM THOSE WITH TRANSFORMER ELEMENTS. RELU - RECTIFIED LINEAR UNIT, GELU - GAUSSIAN ERROR LINEAR UNIT, SGD - STOCHASTIC GRADIENT DESCENT, RMSPROP - ROOT MEAN SQUARE PROPOGATION, BCE - BINARY CROSS-ENTROPY, CE - CROSS-ENTROPY.

Network	Activation Function	Optimizer	Loss Function	Epochs	Learning rate
Unet [28]	ReLU	Adam	BCE	60	1e-3
DeepLabV3 [30]	ReLU	Adam	BCE	60	1e-4
Attn. Unet [29]	Leaky ReLU	SGD	BCE	60	1e-3
PSPNet [31]	Leaky ReLU	RMSProp	Dice	70	1e-4
DAF3D [22]	Leaky ReLU	Adam	Dice + CE	70	1e-4
DenseUnet [33]	Leaky ReLU	Adam	Dice + CE	70	1e-3
UnetR [32]	ReLU	SGD	Dice	60	1e-4
SwinUnet [27]	GeLU	Adam	Dice	80	1e-4
TransUnet [17]	GeLU	Adam	Dice + CE	80	1e-4
SWTR-Unet	GeLU	SGD	Dice + CE	70	1e-4

$$HD(X, Y) = \max\{\hat{H}(X, Y), \hat{H}(Y, X)\} \quad \text{with} \quad (2)$$

$$\hat{H}(X, Y) = \max\{\min\{|x, y|\}\} \quad (3)$$

being the maximum of both directed Hausdorff distances \hat{H} between the two surface point sets X of the reference and Y of the produced segmentation in each direction. \hat{H} was the maximum distance between any point $x \in X$ and their nearest neighbour $y \in Y$ and therefore, represents the worst contour misalignment.

III. RESULTS AND DISCUSSION

The evaluation of the proposed SWTR-Unet consists of three different aspects, which will be discussed successively. First of all, the SWTR-Unet as well as multiple state-of-the-art approaches, that were additionally implemented, were applied to the MRI data. Hence, the segmentation capability of all network variants regarding the liver and its hepatic lesions therein could be compared directly. The second part focuses on the application of the proposed approach to the CT imaging data of the LiTS challenge and therefore, the segmentation accuracy can be assessed on both of the most relevant liver cancer imaging modalities. The final part was conducted to get more insights on potential influencing factors on the segmentation accuracy of the proposed SWTR-Unet, e.g., the number of skip connections and transformer layers or how lesion size or shape influence the segmentation results.

A. MRI-based evaluation

Table II shows the averaged segmentation accuracy of all implemented network variants, including both, multiple state-of-the-art architectures and the proposed SWTR-Unet regarding the liver outline and the hepatic lesions therein. With respect to the entirely convolutional-based network variants, the best results could be achieved with the DenseUnet with on average 96% liver and 74% lesion Dice. Most of the other state-of-the-art CNNs show promising results regarding the liver segmentation, but lack accuracy in terms of the much more challenging segmentation of the hepatic lesions, which would limit any clinical applicability. The observation of some

of the networks producing the worst results revealed several possible reasons for the weak performance: a prevalent cause seems to be false-positive classified pixels in addition to the partly acceptable delineated tumors, which occurs on better performing samples as well but is less pronounced there. This problem is most prominent in the case of Unet and DeepLabV3 (average false-positive rate of 41% and 35% as compared to the 8% of the DAF3D network). Furthermore, these networks are not able to sufficiently segment tumors of irregular shapes. Examples are shown in Figure 4, where the networks' limitations of segmenting non-circular shaped lesions are demonstrated. Similar behavior is observed for tumors of small size, which were not appropriately detected by any of the Unet, Attention Unet, and DeepLabV3 networks. Another challenge for those variants represented tumors located close to the liver surface. In conclusion, the tested convolutional-based networks achieved acceptable segmentation accuracies regarding hepatic lesions of spherical shape, larger size and location in central regions of the liver, but the accuracies drastically decreased for non-spherical shaped and small tumors that are located close to the liver surface. In contrast, transformer-based networks achieved overall higher segmentation accuracies especially regarding the hepatic lesions. The only exception to this was the UnetR variant, which lacked sufficient accuracy for both object classes. The proposed SWTR-Unet variant outperformed any other network in this test in terms of liver and hepatic lesion segmentation, resulting in Dice scores on average of 98% and 81%, respectively. Furthermore, in comparison to most of the state-of-the-art network variants, the proposed SWTR-Unet seemed to widely overcome limitations due to smaller sized and non-spherical shaped lesions.

So far, to the best of the authors' knowledge, there are hardly any published works focusing on deep learning-based hepatic lesion segmentation in MR imaging, except the work of Christ et al. [7], which included MRI data in their otherwise CT-based study. The authors utilized an Unet-style fully convolutional cascaded neural network with a 3D Conditional Random Field (CRF) for the segmentation of the liver and subsequently using the resulting liver mask as an input for the following lesion segmentation. Regarding the MRI part of their work, they trained their network with 38 patient cases and achieved Dice scores on average of 87%

TABLE II

EXPERIMENTAL RESULTS PRODUCED ON THE MRI DATA FOR EACH OF THE TESTED NETWORKS INCLUDING THE PROPOSED SWTR-UNET. STATED ARE THE DICE SIMILARITY COEFFICIENTS (DSC) AND HAUSDORFF DISTANCES (HD) OF THE LIVER AND LIVER LESION SEGMENTATIONS AVERAGED OVER ALL SEVEN FOLDS. THE CENTER LINE SEPERATES PURE CONVOLUTIONAL NETWORKS FROM THOSE WITH TRANSFORMER ELEMENTS.

	DSC		HD	
	DSC_{liver}	DSC_{lesion}	HD_{liver}	HD_{lesion}
Unet [28]	0.93 ± 0.06	0.36 ± 0.38	6.52 ± 9.03	5.49 ± 14.07
DeepLabV3 [30]	0.87 ± 0.10	0.36 ± 0.33	8.35 ± 10.50	9.97 ± 11.66
Attn. Unet [29]	0.91 ± 0.09	0.64 ± 0.29	9.74 ± 9.82	10.07 ± 7.32
PSPNet [31]	0.95 ± 0.01	0.67 ± 0.32	3.04 ± 5.20	17.26 ± 25.82
DAF3D [22]	0.87 ± 0.14	0.73 ± 0.23	18.66 ± 25.43	9.00 ± 22.03
DenseUnet [33]	0.96 ± 0.01	0.74 ± 0.23	1.30 ± 0.98	14.11 ± 26.52
UnetR [32]	0.90 ± 0.07	0.49 ± 0.26	66.49 ± 49.41	34.26 ± 41.81
SwinUnet [27]	0.91 ± 0.14	0.76 ± 0.30	6.32 ± 4.72	4.71 ± 6.77
TransUnet [17]	0.97 ± 0.03	0.76 ± 0.27	1.05 ± 0.23	11.56 ± 25.54
SWTR-Unet	0.98 ± 0.02	0.81 ± 0.28	1.02 ± 0.18	7.03 ± 17.37

for the liver and 69.7% for the hepatic lesion segmentation. Compared to our proposed SWTR-Unet, both segmentations of liver and lesions yielded inferior results of approximately 11%. Furthermore, Christ et al. [7] separated both segmentation task, which results in a dependency on the quality of the preceding liver segmentation step with potential implications with respect to the segmentation accuracy of near-surface tumours in particular. Overall, it could be concluded, that the solely convolutional-based architecture style has its limitations regarding the huge shape, size and location variety, which may not be adequately captured due to the focus of merely local information and features, respectively. Most of the related work regarding hepatic lesion segmentation focused on CT imaging, which will be discussed in the next section. Nevertheless, there are various works addressing MRI-based segmentations of lesions of other organs, e.g., spinal metastases and above all brain lesions [23], [24]. An essential role for a constant enhancement and progress for such specific research issues plays the availability of public grand challenge data, e.g. BRATS [34], since most often the data retrieval is a challenge not to be underestimated.

Additionally, for assessing the quality of the segmentation results, a comparison with the inter-observer variability (IOV) of hepatic lesion segmentations manually produced by experts is instructive. Related literature stated IOV values as Dice scores ranging from 64 – 82% produced on CT images [25]. The proposed SWTR-Unet achieved an average Dice of $81 \pm 28\%$ for hepatic lesions segmentation on MR images, indicating a promising segmentation accuracy on expert level and reasonable applicability in clinical practice. Despite the proposed network, each of the implemented state-of-the-art variants has its limitations with respect to the overall lesion segmentation accuracy.

B. CT-based evaluation

Subsequent to the MRI-based evaluation, the proposed SWTR-Unet was applied to the LiTS challenge CT data (see Table III). On this dataset the proposed network achieved Dice scores on average of $97 \pm 2\%$ for the liver and $79 \pm 25\%$ for the hepatic lesions therein. The mean Hausdorff distances were 2.04 ± 2.30 mm (liver) and 2.44 ± 6.30 mm (lesion).

TABLE III

EXPERIMENTAL RESULTS OF THE PROPOSED SWTR-UNET (PRODUCED ON THE LiTS CHALLENGE CT DATA) IN COMPARISON WITH STATE-OF-THE-ART WORKS. STATED ARE THE DICE SIMILARITY COEFFICIENTS (DSC) OF THE LIVER AND LIVER LESION SEGMENTATIONS.

	DSC_{liver}	DSC_{lesion}
Meng et al. [12]	0.97	0.69
Chlebus et al. [10]	0.96	0.68
Vorontsov et al. [26]	0.95	0.66
Fan et al. [14]	0.96 ± 0.03	0.74 ± 0.08
SWTR-Unet	0.98 ± 0.02	0.79 ± 0.25

There are a few published works focusing on a deep learning-based segmentation of hepatic lesions in CT imaging and since most of them likewise used the LiTS challenge data, a mere direct comparison of the results is possible. Meng et al. [12] experimented with 3D dual-path multi-scale convolutional neural networks. Using this approach, they achieved a Dice of 68.9% for liver tumor segmentation trained on the LiTS dataset. Chlebus et al. [10] presented a 2D convolutional network alongside with an object-based post-processing step to segment the lesions. This network utilized two models to reduce the false positives significantly, in which the first one operates at object level and the second model at voxel level. Chlebus et al. [10] applied their approach to the LiTS challenge data and achieved a mean Dice of 68% for the lesion segmentation. Vorontsov et al. [26] utilized a model consisting of two combined Unet-styled CNNs and also applied their approach to the LiTS challenge data, achieving a mean Dice of 95.1% for the liver and 66.1% for the lesion segmentation. Fan et al. [14] presented a multi-scale attention network, including a self-attention mechanism, that combines local features with global dependencies. Similar to the presented network architecture, they integrated two different attention blocks to achieve this, resulting in mean Dice scores of 96.0% for the liver and 74.9% for the hepatic lesions. They also tested their method on the LiTS challenge data. Compared to these related work, the proposed SWTR-Unet achieved superior results with averaged Dice scores of 98% for the liver and 79% for the hepatic lesions, meaning this novel hybrid network architectures is capable of segmenting the target structures in both, CT and MRI data, while being at the top of or on par

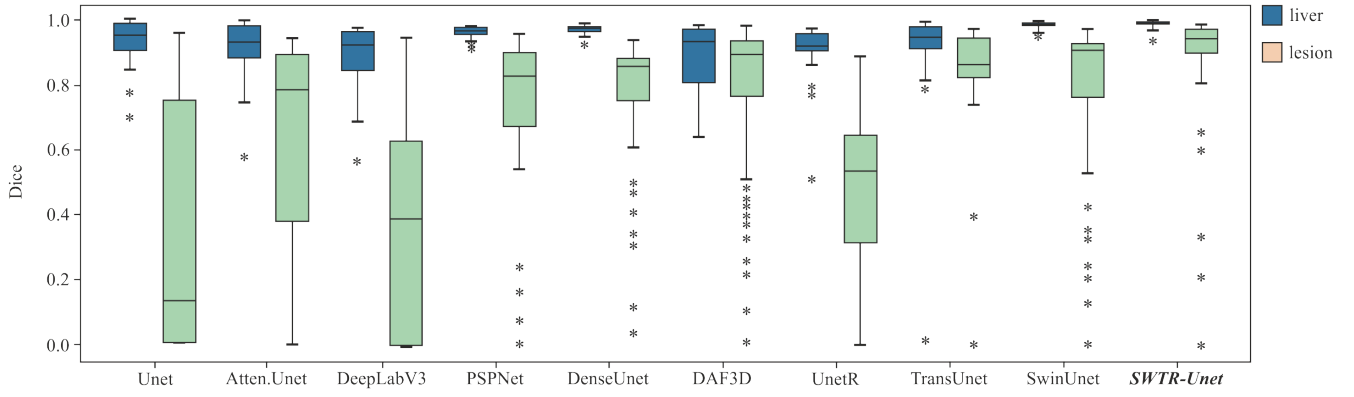


Fig. 3. Resulting Dice similarity coefficients averaged over all folds produced by multiple state-of-the-art network variants as well as from the proposed SWTR-Unet. Box edges mark the 25th and 75th percentiles, the central box line marks the median value and the whisker marks the most extreme values not considered as outliers.

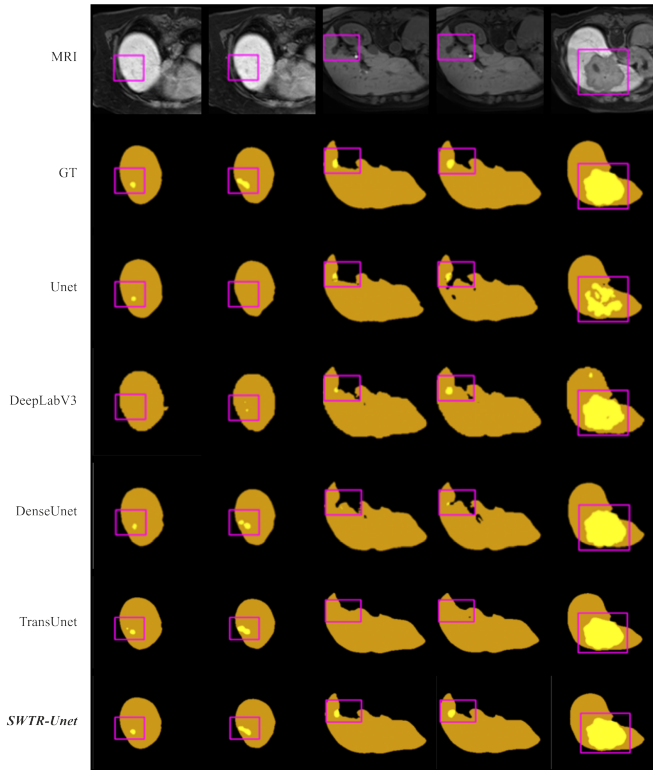


Fig. 4. Shown are five exemplary patient cases (from left to right) of the MRI data with their corresponding ground truth (GT) and the networks' prediction for the liver and lesion mask (from top to bottom) of various state-of-the-art methods as well as the presented SWTR-Unet.

with the state of the art in terms of its segmentation accuracy.

C. Hyperparameter Impact

In order to gain more detailed insights of the performance and corresponding influencing factors of the proposed SWTR-Unet, a number of additional experiments were carried out. Starting with varying the number of skip connections, Table IV, indicates that the segmentation performance increases with growing numbers of skip connections. The thus enhanced ability of the network to capture the lost spatial information during downsampling benefits this effect. Therefore, networks with

a reasonable amount of skip connections will minimize the loss of information and achieve on average better segmentation accuracies.

TABLE IV

SEGMENTATION ACCURACY OF THE SWTR-UNET DEPENDING ON THE NUMBER OF SKIP CONNECTIONS ($\#_{sc}$). STATED ARE AVERAGE AND STANDARD DEVIATION VALUES OF THE DICE SIMILARITY COEFFICIENTS FOR LIVER AND HEPATIC LESION.

$\#_{sc}$	DSC_{liver}	DSC_{lesion}
0	0.89 ± 0.08	0.75 ± 0.15
1	0.91 ± 0.05	0.77 ± 0.19
2	0.95 ± 0.03	0.80 ± 0.22
3	0.98 ± 0.03	0.81 ± 0.27

Table V shows that extending the network from 8 to 12 transformer layers increased the Dice values for both liver and tumor segmentation. Transformer layers are in general beneficial to the segmentation accuracy, since they are suitable for capturing long-range dependencies between pixels and thus, global context information. That means, extending the transformer depth to a certain amount of layer, will likely increase the resulting segmentation accuracy, limited by the drawback of rising computational costs.

TABLE V

SEGMENTATION ACCURACY OF THE SWTR-UNET DEPENDING ON THE NUMBER OF USED TRANSFORMER LAYERS ($\#_{tl}$). STATED ARE AVERAGE AND STANDARD DEVIATION VALUES OF THE DICE SIMILARITY COEFFICIENTS FOR LIVER AND HEPATIC LESION.

$\#_{tl}$	DSC_{liver}	DSC_{lesion}
8	0.94 ± 0.06	0.77 ± 0.17
10	0.97 ± 0.03	0.79 ± 0.14
12	0.98 ± 0.02	0.81 ± 0.28

Furthermore, the impact of the number of training samples on the segmentation quality was examined. This was done by training the network with 25, 30, 35, and 45 randomly selected patients cases and their corresponding 2D slices. It can be seen from Table VI that with an increasing number of training samples, the overall performance of the model could be increased. That should not come as a surprise, since a larger set of independent training data becomes more and

more capable to represent the vast variety of the hepatic lesions' size, shape, and location within the liver and therefore, minimizing overfitting behaviour and leading to an improved generalization capability of the network.

TABLE VI

SEGMENTATION ACCURACY OF THE SWTR-UNET DEPENDING ON THE NUMBER USED PATIENT CASES ($\#_{pc}$) FOR TRAINING PURPOSES. STATED ARE AVERAGE AND STANDARD DEVIATION VALUES OF THE DICE SIMILARITY COEFFICIENTS FOR LIVER AND HEPATIC LESION.

$\#_{pc}$	DSC_{liver}	DSC_{lesion}
25	0.78 ± 0.10	0.60 ± 0.18
30	0.86 ± 0.07	0.72 ± 0.21
35	0.92 ± 0.04	0.76 ± 0.19
40	0.98 ± 0.02	0.80 ± 0.21

D. Correlation analysis

Due to the high variety of shapes, sizes and location of the lesions within the liver, it is of significant interest to examine, how these lesion characteristics affect the segmentation accuracy of the proposed SWTR-Unet and to reveal possible bias. This correlation analysis is again performed on the MRI data. In terms of lesion shape, the ground truth segmentation of all samples was used to determine the lesions' sphericity Ψ by calculating

$$\Psi = \frac{\pi^{\frac{1}{3}}(6V)^{\frac{2}{3}}}{A} \quad (4)$$

with V being the volume and A the surface of the lesion mask. Subsequently, the lesions were divided into two classes, labelling them as spherical ($\Psi > 0.9$, 20 lesions) or merely irregularly shaped ($\Psi < 0.9$, 137 lesions). The experiments clearly indicated higher segmentation accuracies if the lesions were of a mere spherical shape with on average $89 \pm 8\%$ compared to the class of rather irregular shaped lesions with a mean Dice of $72 \pm 20\%$, although these were much more prominently represented in the training set. The prevalence of mere spherical shaped lesions not only increase the chances more accurate segmentations, but benefits also the robustness of the approach as indicated by the significantly lower standard deviation compared to the results of lesions with a $\Psi < 0.9$. The volume V of all lesions derived from the ground truth segmentation was used furthermore to divide the samples into four different lesion size categories, also taking the spatial resolution into account (the volume V of one voxel corresponds to 2.88 mm^3). The results indicate that the averaged segmentation accuracy as well as the robustness of the method increases with larger tumor sizes from $78 \pm 7.6\%$ (size $\leq 1 \text{ cm}^3$, 68 lesions) over $80 \pm 3.1\%$ (size between 1 and 5 cm^3 , 60 lesions) and $82 \pm 2.5\%$ (size between 5 and 10 cm^3 , 17 lesions) to $83 \pm 1.0\%$ (size $\geq 10 \text{ cm}^3$, 12 lesions). This tendency is further consolidated by the fact that the averaged segmentation accuracies of lesions that were categorized into the two classes with the highest volumes achieved better results, although they were severely underrepresented within the training set. Finally, the impact of the lesions' inner hepatic location was examined depending on the distance towards the liver surface. Each lesion was labelled based on the distance d , that is the

closest Euclidean distance between the liver surface and the lesion outline. Therefore, it was differentiated between lesions that were surface-near ($d < 1 \text{ cm}$) or rather centered within the liver ($d > 1 \text{ cm}$). The results indicate, that hepatic lesions close to the liver surface are significantly harder to accurately segment as those, which are more centered within the organ, which is reflected in a remarkably lower mean Dice value of $74 \pm 15\%$ compared to on average $87 \pm 5\%$ for rather centered lesion. This may be caused by the more challenging contrast and texture variety at the liver surface with surrounding other tissues, but could further be attributed to the lower number of such specific training samples (35 surface-near vs. 122 rather centered cases).

IV. CONCLUSION

Precise segmentations of the liver and hepatic tumors is of utmost importance since decisions regarding the proper treatment evermore depend on findings provided by such procedures. Whereas, manual segmentation represents the gold standard in terms of accuracy, it is time-consuming, cumbersome, and unnecessarily ties up valuable resources, which is why automatized procedures gain relevance in clinical settings.

In this work presented a novel hybrid network architecture combining convolutional and transformer-based elements and compared it with additionally implemented state-of-the-art approaches on the same evaluation data. This ensures a direct comparability of all methods, which is otherwise most often limited due to different databases of the related work. In this regard, all network variants were applied to clinical MRI data of the University Hospital of Magdeburg. Furthermore, the proposed approach was applied to publicly available CT imaging data of the LiTS challenge. In order to investigate various influencing factors on the segmentation accuracy, various parameters of the network architecture, as well as the influence of lesion size, shape and location on the results was examined.

Based on these experiments, the proposed SWTR-Unet achieved highly promising segmentation accuracies regarding both, the liver and its hepatic lesions with Dice scores on average of $98 \pm 3\%$ and $81 \pm 25\%$ on MRI and $98 \pm 2\%$ and $79 \pm 25\%$ on CT data. Therefore, to the best of our knowledge, the presented approach outperforms all of the related works and thus, represents the current state of the art. The findings of further experiments underlined the impact of lesion size, shape and location within the liver, which indicated that the segmentation accuracy increases with larger, more spherical and rather centered lesions. Furthermore, it could be shown, that an increasing number of training samples, skip connections and transformer layers have a beneficial effect on the segmentation accuracy. In conclusion, the proposed SWTR-Unet could represent an important step towards a more sophisticated computer-assisted workflow of liver lesion diagnosis and therapy by providing expert-level segmentation accuracy with little to no required user interaction. Therefore, it could support the radiologists in clinical practice by saving valuable resources and time.

REFERENCES

- [1] GBD 2015 Mortality and Causes of Death Collaborators, "Global, regional, and national life expectancy, all-cause mortality, and cause-specific mortality for 249 causes of death, 1980–2015: a systematic analysis for the Global Burden of Disease Study 2015," in *The Lancet*, 388(10053), 2016, pp. 1459–1544.
- [2] T. Heimann, B. van Ginneken, M. A. Styner, Y. Arzhaeva, V. Aurich, C. Bauer, ... and I. Wolf, "Comparison and evaluation of methods for liver segmentation from CT datasets," in *IEEE transactions on medical imaging*, 28(8), 2009, pp. 1251–1265.
- [3] J. Ferlay, H. R. Shin, F. Bray, D. Forman, C. Mathers, and D. M. Parkin, "Estimates of worldwide burden of cancer in 2008: GLOBOCAN 2008," in *International journal of cancer*, 127(12), 2010, pp. 2893–2917.
- [4] G. Li, X. Chen, F. Shi, W. Zhu, J. Tian, and D. Xiang, "Automatic liver segmentation based on shape constraints and deformable graph cut in ct images," in *IEEE Transactions on Image Processing*, 24(12), 2015, pp. 5315–5329.
- [5] C. Li, X. Wang, S. Eberl, M. Fulham, Y. Yin, J. Chen, and D. D. Feng, "A likelihood and local constraint level set model for liver tumor segmentation from ct volumes," in *IEEE Transactions on Biomedical Engineering*, 60(10), 2013, pp. 2967–2977.
- [6] M. G. Linguraru, W. J. Richbourg, J. Liu, J. M. Watt, V. Pamulapati, S. Wang, and R. M. Summers, "Tumor burden analysis on computed tomography by automated liver and tumor segmentation," in *IEEE Transactions on Medical Imaging*, 31(10), 2012, pp. 1965–1976.
- [7] P. Christ, F. Ettlinger, F. Grün, M. E. A. Elshaera, J. Lipkova, S. Schlecht, ... and B. Menze, "Automatic liver and tumor segmentation of CT and MRI volumes using cascaded fully convolutional neural networks," arXiv preprint arXiv:1702.05970, 2017.
- [8] S. Li, G. K. F. Tso, and K. He, "Bottleneck feature supervised U-Net for pixel-wise liver and tumor segmentation," in *Expert Systems with Applications*, 145, 2020, 113131.
- [9] Z. Liu, Y.-Q. Song, V. S. Sheng, L. Wang, R. Jiang, X. Zhang, ... and D. Yuan, "Liver CT sequence segmentation based with improved U-Net and graph cut," in *Expert Systems with Applications*, 126, 2019, pp. 54–63.
- [10] G. Chlebus, A. Schenk, J. Moltz, B. Ginneken, H. Meine, and H. Hahn, "Automatic liver tumor segmentation in ct with fully convolutional neural networks and object-based postprocessing," in *Scientific Reports*, 8(1), 2018, pp. 1–7.
- [11] Q. Jin, Z. Meng, C. Sun, L. Wei, and R. Su, "RA-UNet: A hybrid deep attention-aware network to extract liver and tumor in CT scans," arXiv:1811.01328, 2018.
- [12] L. Meng, Y. Tian, and S. Bu, "Liver tumor segmentation based on 3d convolutional neural network with dual scale," in *Medical Physics*, 21(1), 2020, pp. 144–157.
- [13] X. Li, H. Chen, X. Qi, Q. Dou, C.-W. Fu, and P. A. Heng, "H-denseunet: Hybrid densely connected unet for liver and tumor segmentation from ct volumes," in *IEEE Transactions on Medical Imaging*, 37(12), 2018, pp. 2663–2674.
- [14] T. Fan, G. Wang, Y. Li, and H. Wang, "MA-Net: A Multi-Scale Attention Network for Liver and Tumor Segmentation," in *IEEE Access*, 8, 2020, pp. 179656–179665.
- [15] K. He, X. Zhang, S. Ren, and J. Sun, "Deep residual learning for image recognition," in *Proceedings of the IEEE Conference on Computer Vision and Pattern Recognition*, 2016, pp. 770–778.
- [16] J. Deng, W. Dong, R. Socher, L.-J. Li, K. Li, and L. Fei-Fei, "Imagenet: A large-scale hierarchical image database," in *Proceedings of the IEEE Conference on Computer Vision and Pattern Recognition*, 2009, pp. 248–255.
- [17] J. Chen, Y. Lu, Q. Yu, X. Luo, E. Adeli, Y. Wang, L. Lu, A. L. Yuille, and Y. Zhou, "Transunet: Transformers make strong encoders for medical image segmentation," arXiv preprint arXiv:2102.04306, 2021.
- [18] A. Vaswani, N. Shazeer, N. Parmar, J. Uszkoreit, L. Jones, A. N. Gomez, L. u. Kaiser, and I. Polosukhin, "Attention is all you need," in *Advances in neural information processing systems*, 2017, pp. 5998–6008.
- [19] Z. Liu, Y. Lin, Y. Cao, H. Hu, Y. Wei, Z. Zhang, S. Lin, and B. Guo, "Swin transformer: Hierarchical vision transformer using shifted windows," arXiv preprint arXiv:2103.14030, 2021.
- [20] P. Christ, "LiTS Liver Tumor Segmentation Challenge (LiTS17)," URL <https://competitions.codalab.org/competitions/17094>, 2017.
- [21] P. Bilic, P. Christ, E. Vorontsov, G. Chlebus, H. Chen, Q. Dou, C.-W. Fu, X. Han, P.-A. Heng, J. Hesser, S. Kadoury, T. Konopczyński, M. Le, F. li, X. Li, J. Lipková, J. Lowengrub, H. Meine, J. Moltz, and J. Wu, "The liver tumor segmentation benchmark (lits)," arXiv preprint arXiv:1901.04056, 2019.
- [22] Y. Wang, D. Ni, H. Dou, X. Hu, L. Zhu, X. Yang, M. Xu, J. Qin, P.-A. Heng, and T. Wang, "Deep attentive features for prostate segmentation in 3d transrectal ultrasound," in *IEEE Transactions on Medical Imaging*, 38(12), 2019, pp. 2768–2778.
- [23] G. Hille, M. Dünnwald, M. Becker, J. Steffen, S. Saalfeld, and K. Tönnies, "Segmentation of vertebral metastases in mri using an u-net like convolutional neural network," in *Proceedings of Bildverarbeitung für die Medizin 2019*, 2019, pp. 31–36.
- [24] Z. Jiang, C. Ding, M. Liu, and D. Tao, "Two-stage cascaded u-net: 1st place solution to brats challenge 2019 segmentation task," in *Proceedings of International MICCAI Brainlesion Workshop*, 2019, pp. 231–241.
- [25] E. Vorontsov, M. Cerny, P. Régnier, L. Jorio, C. Pal, R. Lapointe, F. Vandenbroucke-Menu, S. Turcotte, S. Kadoury, and A. Tang, "Deep learning for automated segmentation of liver lesions at ct in patients with colorectal cancer liver metastases," in *Radiology: Artificial Intelligence*, 1(2), 2019, pp. 18014.
- [26] E. Vorontsov, A. Tang, C. Pal, and S. Kadoury, "Liver lesion segmentation informed by joint liver segmentation," in *Proceedings of IEEE 15th International Symposium on Biomedical Imaging (ISBI 2018)*, 2018, pp. 1332–1335.
- [27] H. Cao, Y. Wang, J. Chen, D. Jiang, X. Zhang, Q. Tian, and M. Wang, "Swin-unet: Unet-like pure transformer for medical image segmentation," arXiv preprint arXiv:2105.05537, 2021.
- [28] O. Ronneberger, P. Fischer, and T. Brox, "U-net: Convolutional networks for biomedical image segmentation," in *Proceedings of International Conference on Medical image computing and computer-assisted intervention*, 2015, pp. 234–241.
- [29] O. Oktay, J. Schlemper, L. L. Folgoc, M. Lee, M. Heinrich, K. Misawa, K. Mori, S. McDonagh, N. Y. Hammerla, B. Kainz, B. Glocker, and D. Rueckert, "Attention u-net: Learning where to look for the pancreas," arXiv preprint arXiv:1804.03999, 2018.
- [30] L.-C. Chen, G. Papandreou, F. Schroff, and H. Adam, "Rethinking atrous convolution for semantic image segmentation," arXiv preprint arXiv:1706.05587, 2017.
- [31] H. Zhao, J. Shi, X. Qi, X. Wang, and J. Jia, "Pyramid scene parsing network," in *Proceedings of the IEEE conference on computer vision and pattern recognition*, 2017, pp. 2881–2890.
- [32] A. Hatamizadeh, D. Yang, H. Roth, and D. Xu, "Unetr: Transformers for 3d medical image segmentation," in *Proceedings of the IEEE/CVF Winter Conference on Applications of Computer Vision*, 2022, pp. 574–584.
- [33] S. Cai, Y. Tian, H. Lui, H. Zeng, Y. Wu, and G. Chen, "Dense-UNet: a novel multiphoton in vivo cellular image segmentation model based on a convolutional neural network," in *Quantitative imaging in medicine and surgery*, 10(6), 2020, pp. 1275.
- [34] B. H. Menze, A. Jakab, S. Bauer, J. Kalpathy-Cramer, K. Farahani, J. Kirby, et al. "The Multimodal Brain Tumor Image Segmentation Benchmark (BRATS)," in *IEEE Transactions on Medical Imaging*, 34(10), 2015, pp. 1993–2024.